

# RF-Harvesting Tightly Coupled Rectenna Array Tee-Shirt With Greater Than Octave Bandwidth

José Antonio Estrada<sup>1</sup>, *Member, IEEE*, Eric Kwiatkowski<sup>2</sup>, *Member, IEEE*, Ana López-Yela<sup>3</sup>,

Mónica Borgoñós-García, Daniel Segovia-Vargas<sup>4</sup>, *Member, IEEE*,

Taylor Barton<sup>5</sup>, *Senior Member, IEEE*,

and Zoya Popović, *Fellow, IEEE*

**Abstract**—This article presents 16- and 81-element broadband rectenna arrays screen printed on a cotton tee-shirt for harvesting 4–130- $\mu\text{W}/\text{cm}^2$  power densities between 2 and 5 GHz. A packaged SMS7630-079LF Schottky diode is connected with silver paint and soldered to each element of the array. The diode impedance over frequency as a function of dc load and input power is analyzed using source-pull harmonic-balance simulations. The antenna is a quasi-self-complementary tightly coupled bow-tie array with a period of about  $\lambda_0/6$  at the highest frequency. The impedance at the element ports of the array and the array radiation pattern are analyzed with source-pull diode complex impedance port terminations. Full-wave simulations are performed with the cotton fabric on top of specific tissue layer stack-up for a human torso, as well as for a body phantom. Measurements using a water-filled phantom show up to  $P_{\text{dc}} = 32 \mu\text{W}$  for incident power densities of  $4 \mu\text{W}/\text{cm}^2$ , with a dc load of  $R_{\text{dc}} = 2 \text{ k}\Omega$ . At higher incident power density levels of  $100 \mu\text{W}/\text{cm}^2$ , up to 32% efficiency is measured. Measured rectified voltage and efficiency for the wearable tee-shirt are in good agreement with phantom measurements for the 81-element array. In addition, the effects of body curvature, air layer between tee-shirt and skin, and washing of the fabric are quantified in either simulation or measurements.

**Index Terms**—Energy harvesting, rectenna, Schottky, screen printed, tee-shirt, wearable.

Manuscript received November 14, 2019; revised February 13, 2020; accepted March 23, 2020. Date of publication May 11, 2020; date of current version September 2, 2020. The work of José Antonio Estrada was supported in part by the Electronic Materials Interdisciplinary Research Track. The work of Eric Kwiatkowski was supported by the Dean's Graduate Assistantship in the College of Engineering, University of Colorado. The work of Ana López-Yela was supported by the Spanish Ministry of Education, Culture and Sport for University Teacher Training (FPU) and the project TEC2016-80386-P. The work of Zoya Popović was supported by the Lockheed Martin Endowed Chair at the University of Colorado Boulder. This article is an expanded version from the IEEE Wireless Power Transfer Conference 2019 titled “An Octave Bandwidth RF Harvesting Tee-Shirt”, London, U.K., June 17–21, 2019. (*Corresponding author: José Antonio Estrada.*)

José Antonio Estrada, Eric Kwiatkowski, Taylor Barton, and Zoya Popović are with the Department of Electrical, Computer, and Energy Engineering, University of Colorado at Boulder, Boulder, CO 80309 USA (e-mail: jose.estrada@colorado.edu).

Ana López-Yela, Mónica Borgoñós-García, and Daniel Segovia-Vargas are with the Department of Signal Theory and Communications, Universidad Carlos III de Madrid, 28911 Madrid, Spain (e-mail: anlopezy@ing.uc3m.es).

Color versions of one or more of the figures in this article are available online at <http://ieeexplore.ieee.org>.

Digital Object Identifier 10.1109/TMTT.2020.2988688

0018-9480 © 2020 IEEE. Personal use is permitted, but republication/redistribution requires IEEE permission.

See <https://www.ieee.org/publications/rights/index.html> for more information.

## I. INTRODUCTION

WEARABLE devices for fitness and sports, entertainment, health care, defense, and industrial monitoring are gaining popularity, as companies such as Apple, Fitbit, Adidas, Garmin, Nike, Google, Samsung, Sony, and so on are placing more devices on the market daily. In 2020 the global wearable devices market is expected to exceed US\$77.3 billion by 2025 according to some market studies. The devices include foot, wrist, eye, neck, and body wear, and many include wireless functions thus requiring antennas. For example, a  $2 \times 2$  MIMO antenna for 5G is demonstrated in a wrist watch with greater than 85% efficiency [1].

In this article, simulations and measurements are presented for a wearable screen-printed active antenna array shown in Fig. 1(a). The antennas' couple-harvested microwave broadband radiation to an array of rectifiers, providing power for low-power wearable wireless sensors. The self-complementary, tightly coupled bow-tie array is geometrically similar to the nonwearable design in [2]. The period of the array is 1.25 cm, which is approximately  $\lambda_0/6$  at the highest frequency considered in the measurements. Each array element feed is connected to a packaged Schottky diode using silver paint and solder.

Wearable antennas related to on-body telemetry include implantable wireless capsule endoscopy, insole shoe monitoring, and eyeglass frame monitoring sensors [3]–[5]. Different materials amenable to antenna integration are under investigation. In [6], a silver-coated nylon ripstop fabric patch antenna with detachable radiating elements is presented, while [7] demonstrates embroidered antennas with pcb resolution. Antenna integration is demonstrated in denim [8], as well as military berets for GPS, fabricated on a conductive metallized nylon fabric over a felt substrate [9]. In [10], a UHF RFID tag was tested over the human body after several washing and drying cycles of a cotton tee-shirt, and screen-printed antennas with washing effects are presented in [11]. Extensive characterization of different textile materials for wearable antennas is described in [12], and a comparison of various technologies in [13] and [14], where challenges associated with soldering electronic devices to conductive textile patterns are highlighted.

Antennas integrated with rectifiers, or “rectennas,” were developed in the 1950s and there are many excellent reviews

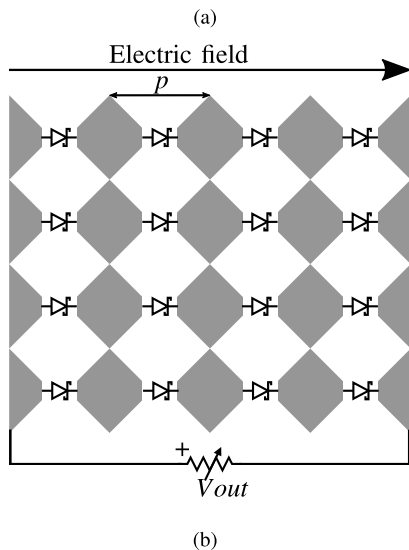
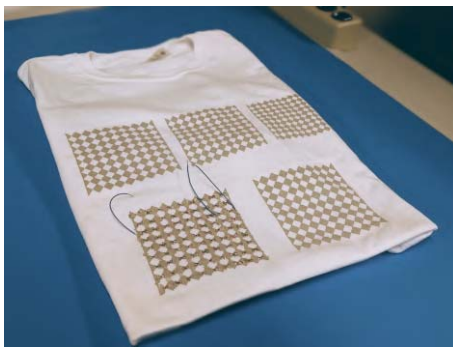


Fig. 1. (a) Photograph of RF harvesting tee-shirt with several screen-printed rectenna arrays. (b) Circuit diagram of a  $4 \times 4$  subarray showing the Schottky diode connections to a dc load that represents the electronic application. The period ( $p$ ) of the array is much smaller than a wavelength and is about  $\lambda_0/6$  at the highest frequency of operation. The horizontal polarization is referred to as the copolarized, consistent with diode orientation.

of this topic [15]. Wearable rectennas include dual-polarized screen-printed patches on cotton substrates [16], a 2.45-GHz patch antenna and array on a cordura fabric for power levels down to  $-40$  dBm [17], and a 2.45-GHz textile patch for watt-level incident power [18], and a UHF patch on a bilayer jeans substrate [19]. In addition to these narrowband rectennas, some broadband implementations have been demonstrated, for example, a 0.9–4-GHz circularly polarized archimedean spiral [20], and a 0.5–8-GHz logarithmic spiral embroidered with conductive yarn into denim [21].

Harvesting ambient RF power has been of interest for powering low duty-cycle sensors for several decades [22]–[24]. Applications for harvesters range from powering aircraft sensors from altimeter antenna sidelobes [25] to multiband rectennas integrated in a kitchen quartz clock and environmental sensor [26], as well as wearable devices that can harvest multiple frequencies [27]. The incident power densities are typically variable and in the range of  $1$ – $10 \mu\text{W}/\text{cm}^2$ , as quantified in an urban environment in [28]. Several rectennas for power densities of  $1 \mu\text{W}/\text{cm}^2$  have been demonstrated with efficiencies greater than 30%, including a 2-g design on a flexible substrate [29] and a directive antenna with an unconventional reflector [30]. In a harvesting scenario when

incident power densities can vary over a wide range, the rectifier element impedance at the fundamental frequency varies dramatically [31]. Codesign of the rectifying element and dual-polarized antennas is discussed for a 2-GHz narrowband rectenna in [32] and for a 2–18-GHz broadband spiral array in [22]. At these low power levels, integrated design of the rectifier, antenna, and power management circuit has been shown to result in the highest efficiency, requiring extensive rectenna characterization as a function of the dc load [33].

In this article, we present a study related to the wearable bow-tie rectenna array beyond the contents in [34]. Section II presents spectrum measurements which give us an idea of the available power density levels, polarization content, and variation over time for RF energy harvesting. This motivates the rectifier diode choice, as described in Section III with source-pull nonlinear simulations. Section IV presents a study of the tightly coupled bow-tie antenna array placed on tissues corresponding to a human torso, as well as a phantom used in measurements. Section V discusses rectenna array fabrication and measurement setups followed by measurement results. The rectenna array is characterized on a water phantom as well as on a human body. On-body measurements are performed to characterize the array in the context of wearable RF-harvesting clothing.

## II. AMBIENT CHARACTERIZATION FOR RF HARVESTING

To inform rectifier design, knowledge of the available incident power density levels, as well as their variation over time, is required. We therefore performed electric-field measurements indoor in two laboratories and outdoor on the roof of a building. A calibrated Keysight N6850A broadband omnidirectional antenna operating from 0.5 to 5 GHz was used with a N9918A FieldFox 26.5-GHz handheld microwave analyzer for collecting the data presented in Fig. 2.

The field measurements are calibrated using the antenna factor provided by the manufacturer. It is defined by the ratio of the magnitude of the electric-field incident on the antenna to the voltage at the  $50\text{-}\Omega$  antenna port and expressed in V/m, or  $\text{dB}\mu\text{V}/\text{m}$  [35]. Measurements were taken in two linear orthogonal polarizations (horizontal and vertical) every 30 s over 1004 frequency points. With a resolution bandwidth of 10 kHz, the measurements were averaged over three hours during a normal week day.

In Fig. 3, the minimum and maximum electric-field values measured at each considered scenario are presented to show the variation of field levels. The frequency bands over which the power density was measured are 0.5–1, 1.5–2, and 2–2.5 GHz. The data show that it is possible to harvest RF energy in the sub-6-GHz range in current electromagnetic environments. As more wireless devices are connected in sub-6-GHz 5G bands (FR1) [38], it is expected that these levels will increase. Therefore, we investigate a frequency range above 2 GHz to include the highest band in Fig. 3 and extend the harvesting frequencies to an octave above it.

The measured electric-field values shown in Figs. 2 and 3 corresponds to power densities up to  $S = E^2/120\pi = 3 \mu\text{W}/\text{cm}^2$  in a single polarization at one frequency. To obtain

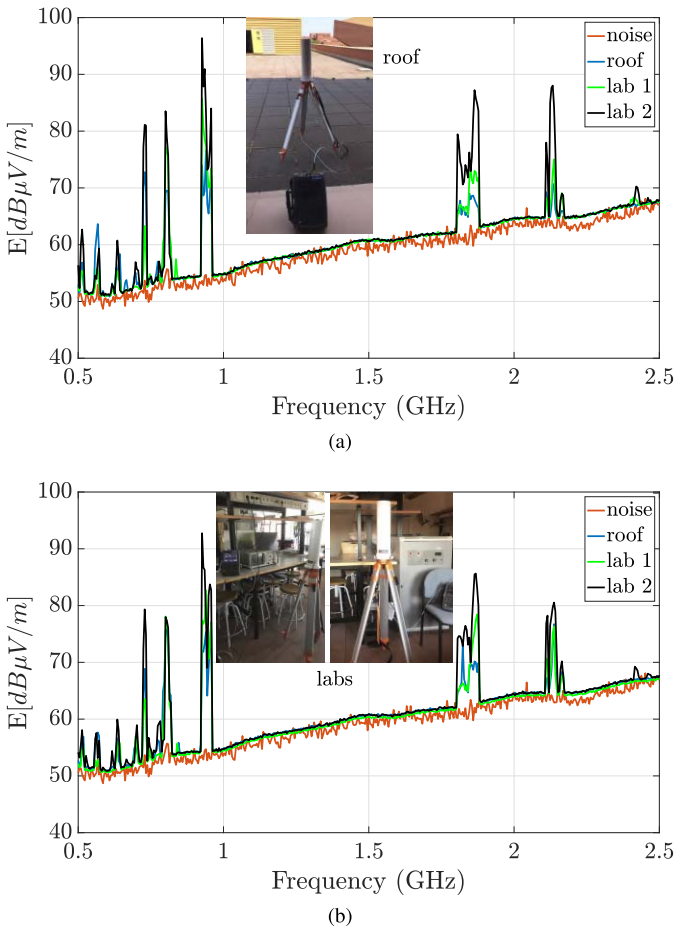


Fig. 2. Electric field measurement for three different scenarios: outdoor [at the roof of the building, shown in inset of (a)] and indoor [at two different laboratories, shown in inset of (b)], for (a) horizontal polarization and (b) vertical polarization.

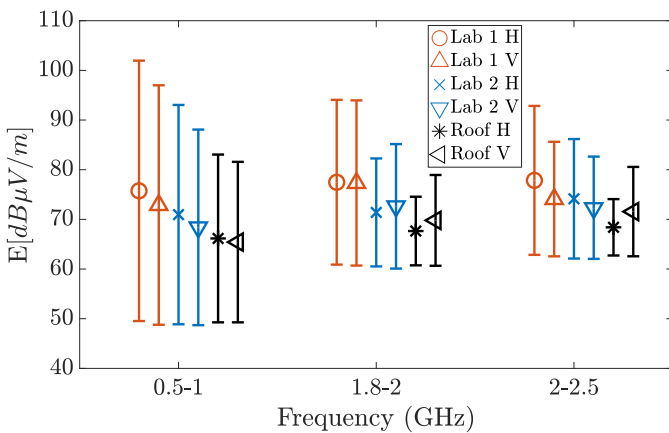


Fig. 3. Variation of measured electric-field values over time for the considered frequency bands for the three measured sites, in both horizontal and vertical polarizations. The measurements are taken every 30 s over 3 h with a 10-kHz resolution bandwidth.

the total power density, these values are integrated over frequency and polarization. Acknowledging that it is unlikely that a Schottky diode rectifier will turn on at the lowest field levels, a few  $\mu\text{W}/\text{cm}^2$  was used as a starting point for the wearable rectenna design, as described in Section III. It is noted that

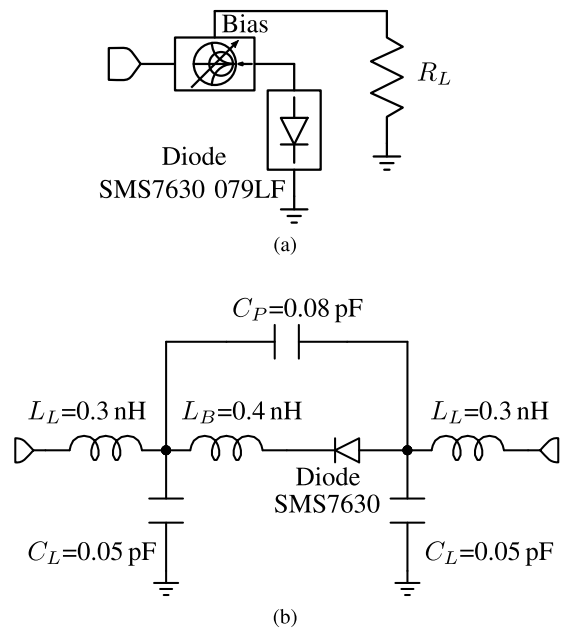


Fig. 4. Circuit schematic for diode simulations (performed in NI/AWR). (a) Source-pull setup and (b) diode package (SC-79 or SOD523) model taken from the application note [36] for use with the diode SPICE model [37].

these values are well below the safety recommendations for general public exposure given by the International Commission on Non-Ionizing Radiation Protection (ICNRP) [39].

### III. DIODE RECTIFIER SIMULATIONS

We next describe simulations of a single-ended diode rectifier based on a commercially available Schottky diode, over a range of power levels, frequencies, and dc loads. The determined diode impedance for best efficiency can then be used to design a broadband antenna array. A Skyworks SMS7630-079LF zero-bias Schottky diode [37] is selected as the rectifying element and is characterized using nonlinear harmonic balance simulations in NI/AWR over a range of expected frequencies and incident power densities. In [25], this diode is compared to several other commercially available packaged diodes in the 4-GHz range, while in [22] it is shown to have the highest efficiency of several commercial diodes for the incident power levels and frequency range used here.

The simple source-pull analysis schematic is shown in Fig. 4(a), where the tuner also presents a dc block and the input power, frequency, and dc load are varied. Fig. 4(b) shows the diode model with parasitics [36] used in the harmonic balance simulations. A range of RF impedances that the antenna should present for best rectification efficiency across a fixed 2-k $\Omega$  load is shown in Fig. 5(a) with contours of constant output dc power for a fixed input power of 100  $\mu\text{W}$  at 2 and 5 GHz, the edges of the frequency band.

Fig. 5(b) shows the impedance obtained from diode source-pull for best efficiency at peak dc output power for varying frequencies and dc load. This determines the approximate range of impedances that the antenna needs to present over a broad frequency and input power density range for best rectification efficiency. Fig. 6 shows the rectified power versus

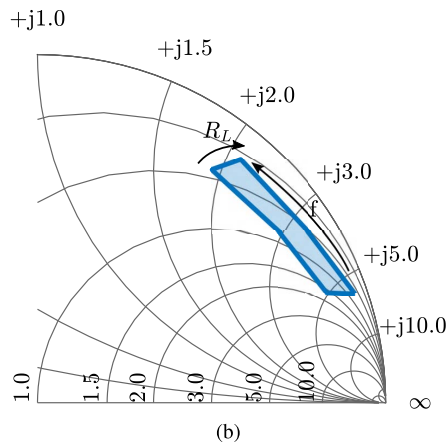
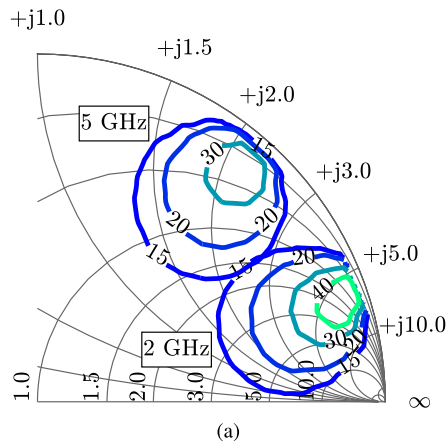


Fig. 5. (a) Simulated source-pull results showing contours of constant rectified power (in  $\mu\text{W}$ ) at 2 and 5 GHz with an input power and dc load of  $100 \mu\text{W}$  and  $2 \text{ k}\Omega$ , respectively. (b) Region of optimum impedance to present to the diode for peak dc output power, obtained using source-pull, showing the trend in frequency ( $f$ ) and load ( $R_L$ ).  $f$  is swept from 2 to 5 GHz while  $R_L$  goes from 500 to  $3000 \Omega$  and the input RF power is  $100 \mu\text{W}$ .

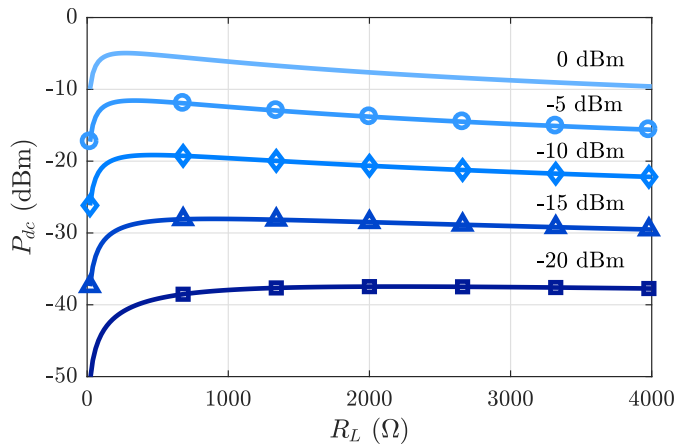


Fig. 6. Simulated rectified dc output power versus dc load resistance  $R_L$  for various RF input powers. The maximum occurs at around  $2 \text{ k}\Omega$  at the lowest input power level.

dc load for several incident powers close to the center of the band at 2.9 GHz. The frequency band under consideration for this article ranges from 2 to 5 GHz. At the lowest power level, the best rectification efficiency occurs for a  $2\text{-k}\Omega$  dc load.

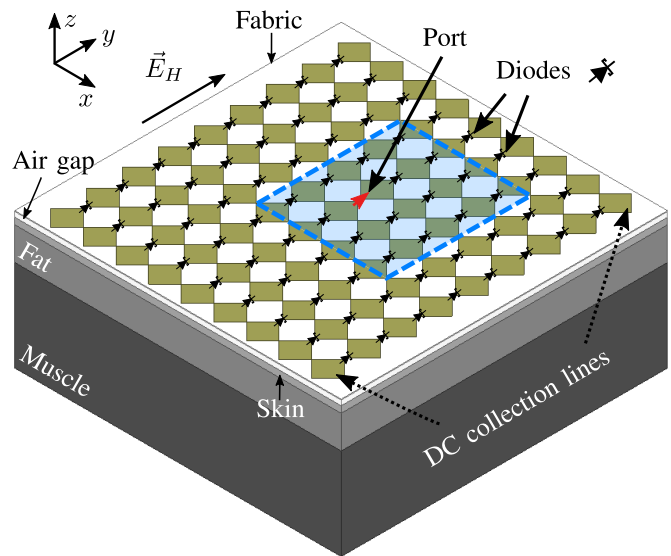


Fig. 7. Simulation geometry for  $9 \times 9$  array showing tissue stackup, orientation (horizontal polarization shown as  $\vec{E}_H$ ), diodes in each element, and main port for impedance and radiation pattern simulations. The  $4 \times 4$  element subarray is highlighted in dashed lines.

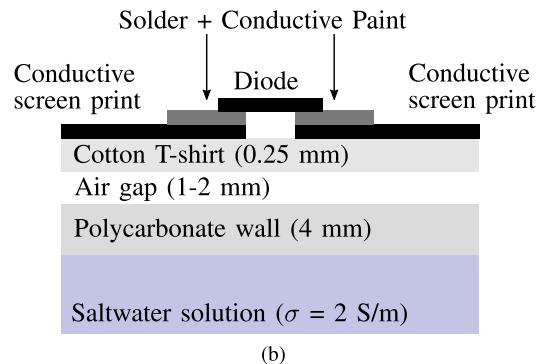
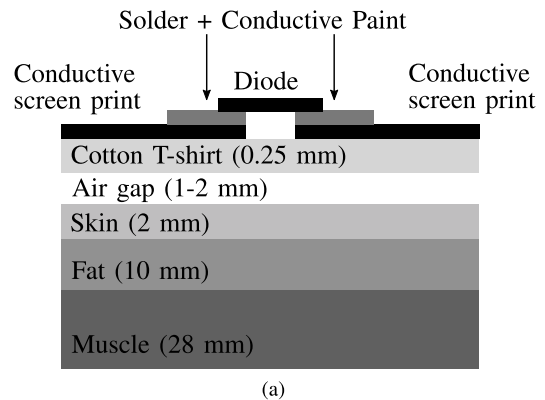


Fig. 8. (a) Cross Section of realistic body tissue stackup with rectenna on tee-shirt placed on top of the model. The relative permittivities and conductivities of the skin, fat, and muscle are 39.7, 5.4, 54.1 and 1.035, 0.064, 1.142 S/m, respectively, and are taken from [41]. (b) Stackup of the water phantom model to aid in measurement repeatability.

At increased power, the best load is around a few hundred ohms. We therefore chose a  $2\text{-k}\Omega$  load which is the best value for the lowest power level, efficient maximum power point

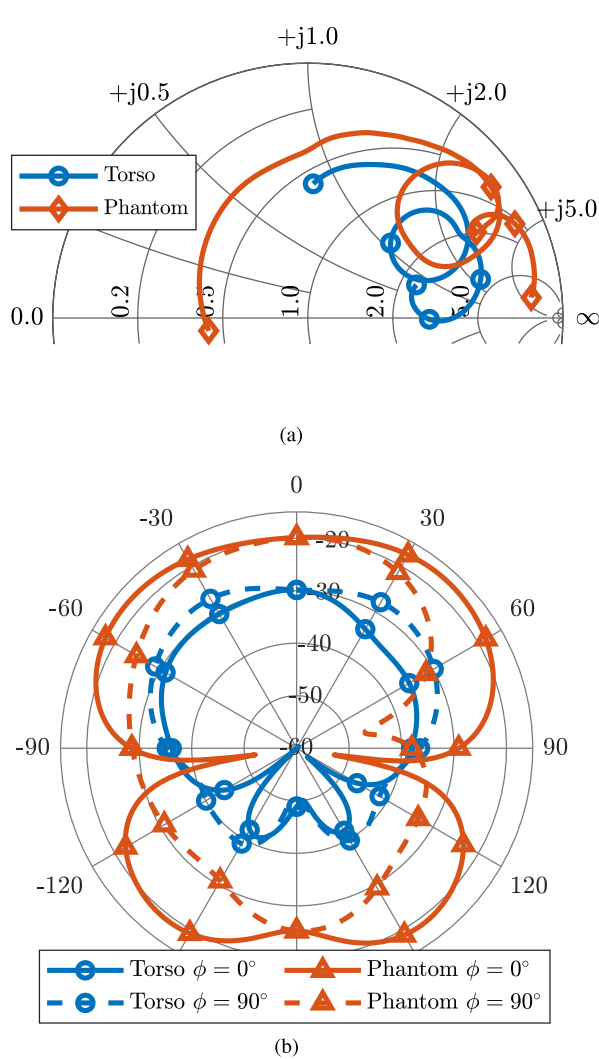


Fig. 9. Simulated results for the antenna with a single feed in the middle of a 16-element array and for two cases: on-phantom and on-body (skin, fat and muscle) with all other feed points terminated in the complex impedance of the diode. (a) Simulated antenna impedance seen at the port labeled in Fig. 7 from 2 to 5 GHz. (b) Antenna radiation pattern gain (realized) at 2.9 GHz.

tacking (MPPT) can be used to dynamically vary this load in a practical setting [40].

#### IV. ANTENNA ARRAY SIMULATIONS

Because of the large incident power variation and broad bandwidth, a tightly coupled quasi-self-complementary antenna array loaded with rectifiers is chosen with a period of  $\lambda_0/6$  at 5 GHz, as shown in Fig. 1(b). The diodes are connected to the antenna feed points in series along the copolarized electric field vector and the rows are connected in parallel to the dc load. The antenna elements are tightly coupled to average out the variations across frequency, power, and shape, making the array an equivalent active impedance sheet. The antenna array is simulated using CST and several cases are compared. The general simulation geometry is shown in Fig. 7.

We show results with  $4 \times 4$  and  $9 \times 9$  finite square arrays of equal periodicity. For wearable applications, the tee-shirt is placed on a realistic body torso tissue stackup

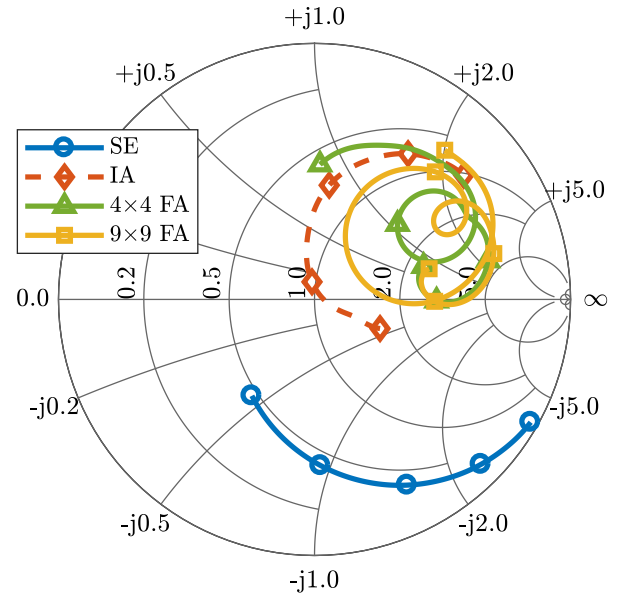


Fig. 10. Driving-point impedance for a SE, an IA and two FAs of  $4 \times 4$  and  $9 \times 9$  elements over a torso with air gap  $h = 1$  mm. Each element is loaded with the complex impedance of the diode and the array impedance is for the center element. The frequency is swept from 2 to 5 GHz.

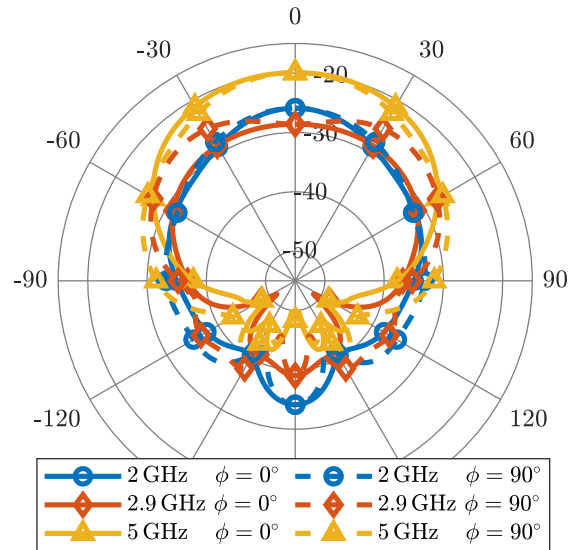
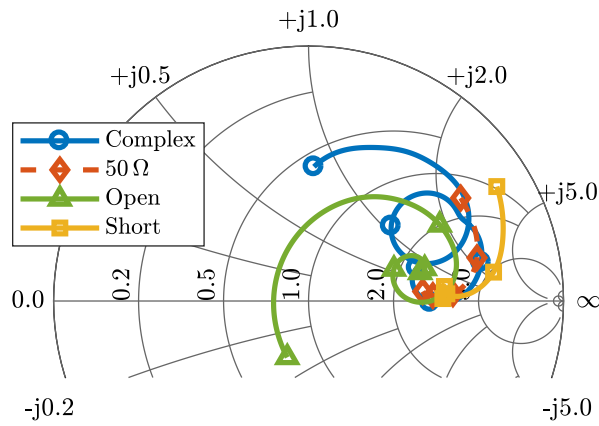


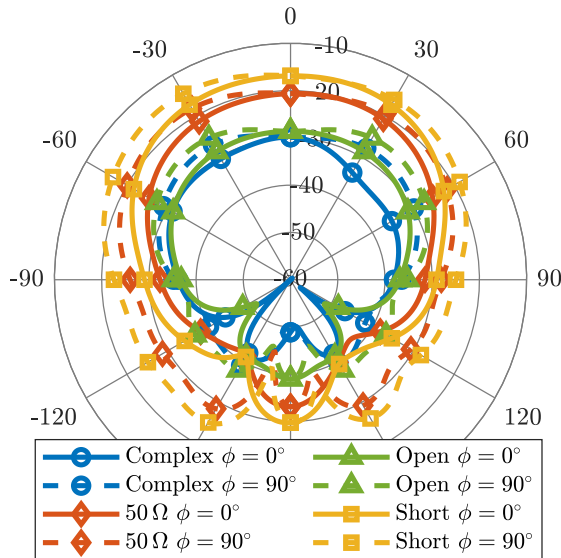
Fig. 11. Simulated copolarized ( $\phi = 0^\circ$ ) and cross-polarized ( $\phi = 90^\circ$ ) gain patterns (realized) for the  $4 \times 4$  array on cotton above an air layer of 1 mm and torso tissue stackup. The center element is fed, while the remaining elements are terminated in the diode impedance.

in the simulations, with a cross Section shown in Fig. 8(a). Measurements are performed on a phantom for repeatability, thus the simulations are also performed for the stackup of a water phantom [Fig. 8(b)].

The impedance and gain of the center element of a finite array (FA) on lossy tissues and phantom model are compared in Fig. 9. Fig. 9(a) displays the input impedance of a  $4 \times 4$  element array simulated over a phantom and over a torso tissue stackup. The diode impedance is modeled from 2 to 5 GHz as a series  $RLC$  network where  $R = 0.1 \Omega$ ,  $L = 0.423$  nH, and  $C = 0.27$  pF. It is noted that the impedances for the



(a)

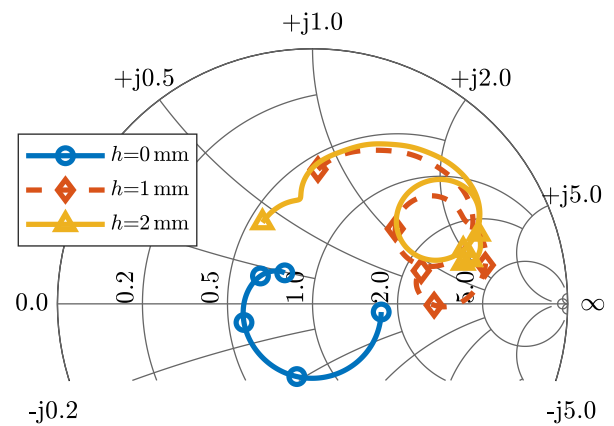


(b)

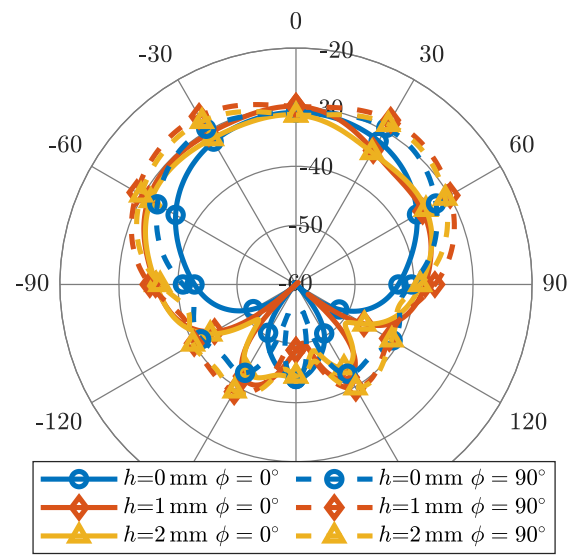
Fig. 12. Simulation results of a  $4 \times 4$  array over a torso with a 1-mm air gap between the cotton and skin layers, with various port terminations. (a) Input impedance looking into a single port (as shown in Fig. 7) from 2 to 5 GHz. (b) Radiation pattern gain (realized) at 2.9 GHz.

center element for the phantom and torso tissue stackup are not identical, but are in the same region of the Smith chart with a similar resonance, indicating that the phantom is a good qualitative model for this tissue stack-up. In Fig. 9(b), the radiation patterns for these cases at 2.9 GHz are shown. The asymmetry of the radiation pattern is due to the offset position of the feed element in a  $4 \times 4$  array, as indicated in dashed line in Fig. 7.

Fig. 10 shows the driving-point impedance from 2 to 5 GHz of the middle element in the two FAs ( $4 \times 4$  and  $9 \times 9$ ), an infinite array (IA), and a single element (SE). In the case of the arrays, the plot shows the impedance of the driven element from Fig. 7, where the other elements are loaded with the input impedance of the diode. It is noted that the SE impedance is capacitive and consistent with that of a thick dipole, while the impedance of the arrays is significantly different, due to the electrically small period that results in tight coupling. Also it is noted that the impedance of the larger array is closer to that of the IA, as expected.



(a)



(b)

Fig. 13. Simulation results of a  $4 \times 4$  array over a torso loaded with the complex impedance of the diode for various air gaps ( $h$ ). (a) Input impedance looking into a single port (as shown in Fig. 7) from 2 to 5 GHz. (b) Radiation pattern gain (realized) at 2.9 GHz.

Fig. 11 shows the simulated gain patterns for a  $4 \times 4$  array on cotton above a torso tissue stackup with a 1-mm air layer between the shirt and the skin. The center element is fed, while the remaining elements are terminated in the diode impedance. The patterns are shown for three frequencies across the band. The highest gain is observed at the upper end of the band where the coupling is the weakest. Back radiation is greater at lower frequencies due to the electrical dimension of the finite substrate and tissue stackup.

Fig. 12 shows the input impedance and radiation pattern of a  $4 \times 4$  array over a torso with 1-mm air gap for various terminations on the other ports, in this case an open, short,  $50\text{-}\Omega$  load and the complex impedance of the diode. The short and  $50\text{-}\Omega$  terminations produce similar results because the  $50\text{-}\Omega$  loads are a small impedance and closer to the short than to the diode and antenna impedance magnitudes, which are in the hundred ohm range. Likewise, the open and diode impedances produce similar results in both impedance and

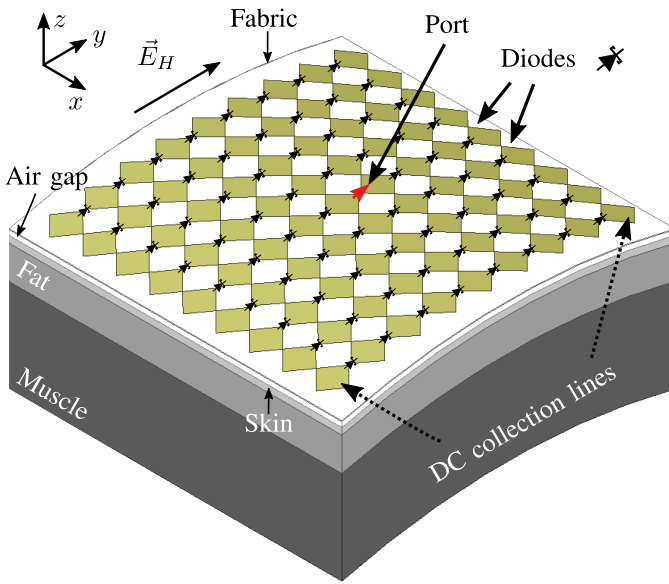


Fig. 14. Simulation geometry for a curved  $9 \times 9$  array showing tissue stackup, orientation (horizontal polarization shown as  $\vec{E}_H$ ), diodes in each element, and main port for impedance and radiation pattern simulations. The array is deformed in a cylindrical manner with the axis along the  $x$ -direction, a radius of curvature of 319 mm, and a  $30^\circ$  angle.

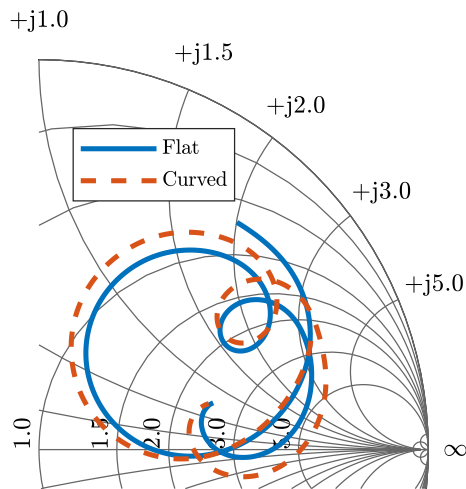


Fig. 15. Comparison of input impedance looking into a single port (as shown in Fig. 14) from 2 to 5 GHz for flat and curved arrays when the rest of the elements are loaded with the diode complex impedance.

radiation pattern. The different terminations are included to point out the impact of port terminations in a tightly coupled array. We believe that the complex diode impedance terminations are the most appropriate to use in this case, although they are incident power, frequency, and load dependent as shown in Fig. 5(b).

Since clothing tends to be loose, the spacing between the cotton tee-shirt and skin will vary in general. We therefore examine the impedance and pattern dependence on the thickness of the air layer as a first-order approximation. Fig. 13

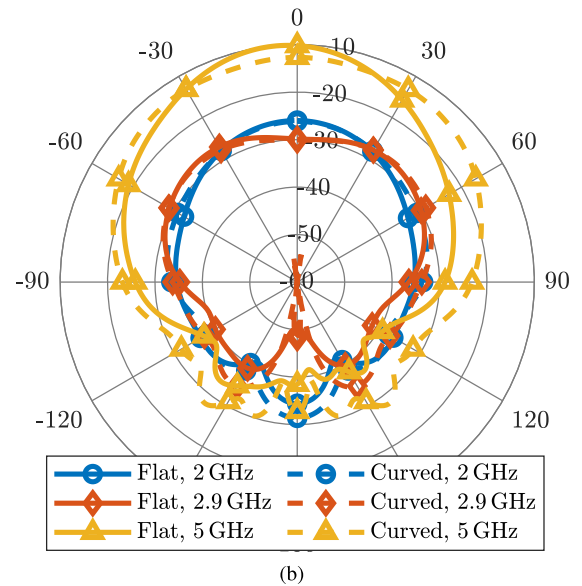
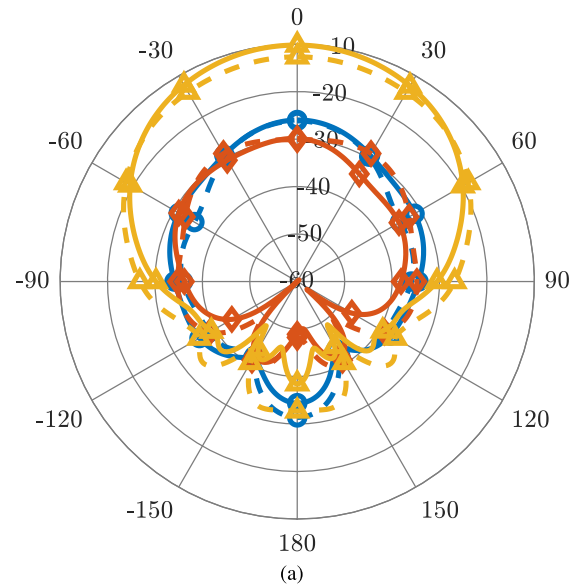


Fig. 16. Comparison of realized gain for a flat and a curved array. (a) Copolarized ( $\phi = 0^\circ$ ). (b) Cross-polarized ( $\phi = 90^\circ$ ).

shows the simulated input impedance and radiation pattern of the same array as Fig. 12 with varying air gap ( $h$ ). The performance of the array does not vary much from 1 to 2 mm but it does change when the gap is reduced or disappears. This suggests that on materials such as fleece or other thicker fabrics, the variation would not be noticeable.

Another practical consideration is the effect of curvature of various parts of the body. A simulation of the rectenna curved with a radius of 319 mm extending over  $30^\circ$  is performed for the  $9 \times 9$  array with a 1-mm air gap, as illustrated in Fig. 14. The resulting driving-point impedance of the center element, with complex loads terminating the rest of the ports, is shown in Fig. 15. The radiation pattern comparisons are shown in Fig. 16. Only a small shift in performance is seen, and the curved array has more side radiation with a small reduction in the main lobe maximum.

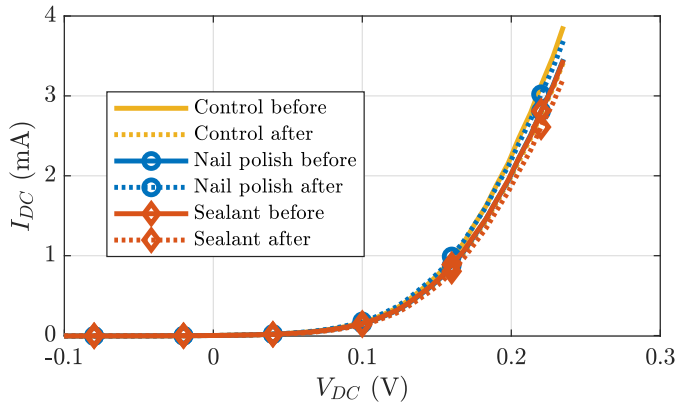


Fig. 17. Comparison of  $I$ - $V$  curves for different treatments before and after hand washing.



Fig. 18. Photograph of tee-shirt on phantom in the anechoic chamber during measurements, with the phantom shown on the bottom right. A detail of a fabricated single array element is shown on the top right.

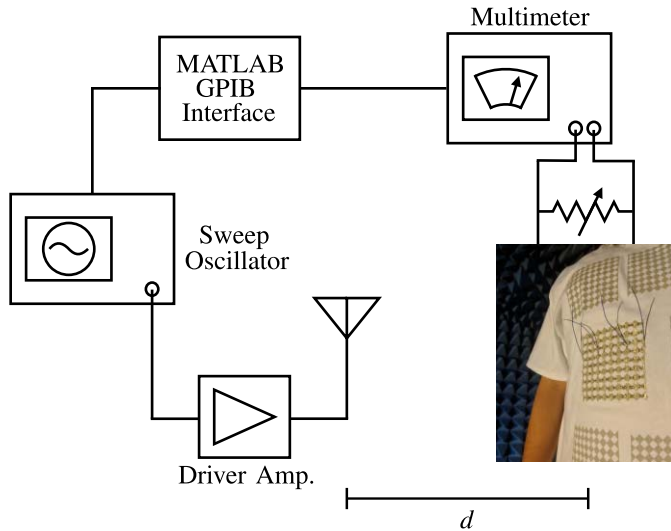
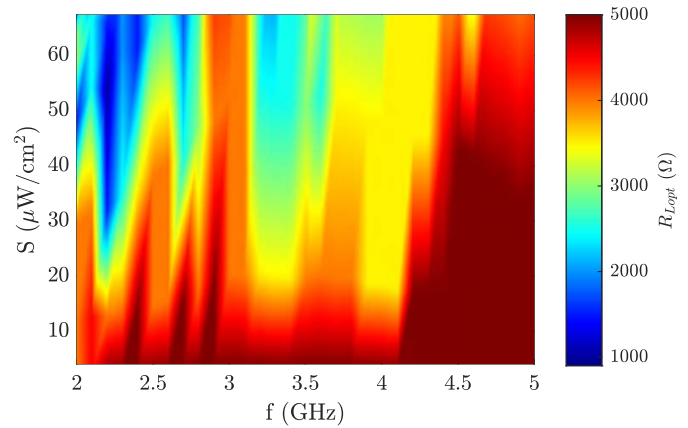


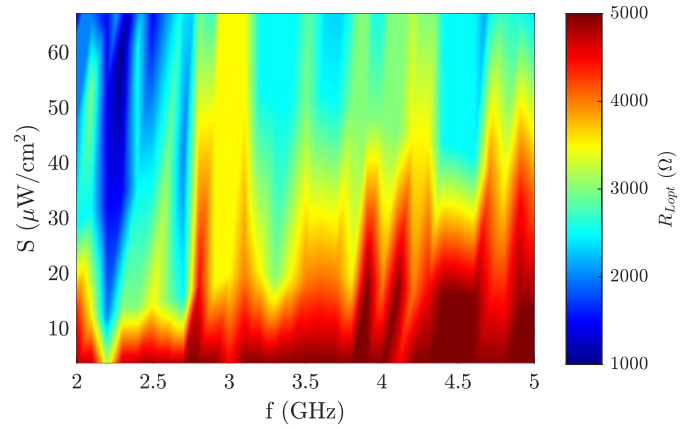
Fig. 19. Measurement setup,  $d = 69$  cm. The tee-shirt is measured inside of an anechoic chamber in several configurations: mounted in air (free space), on a phantom, and while being worn (on-body). The calculated far-field distance,  $d_f$ , is approximately 26 cm at 2 GHz.

V. IMPLEMENTATION AND MEASUREMENTS

To implement the bow-tie array on wearable material, metallized ink (NovaCentrix Metalon HPS-FG57B) is deposited



(a)



(b)

Fig. 20. Optimum load resistance for the 81-element array in (a) vertical and (b) horizontal polarization.

on a cotton tee-shirt using standard screen printing [42] methods. The surface-mount diode package (SC-79) proved to be difficult to attach to the conductive ink using solely solder or conductive epoxy. An adhesion method was developed which utilizes conductive silver paint that was then soldered to following curing of the paint. The temperature of the soldering iron was maintained at 375°C during this process. The surface resistance of the silver paint is 0.01  $\Omega/\square$ , which maintains greater performance in terms of repeatability and low resistance due to lower viscosity of the paint when compared with that of conductive epoxy.

To investigate effects of fabric washing, three diodes were mounted in unit cells on a different Tee-shirt and without connections between them. One was then covered with nail polish and a second one with fixative spray for pastels and charcoal drawings (by Grumbacher). Both materials are resistant to washing. The  $I$ - $V$  curves of all three diodes were measured before and after hand washing in water, and there was no observable change in dc electrical characteristics (see Fig. 17).

A  $4 \times 4$  array was initially populated with diodes and characterized and then expanded to a  $9 \times 9$  array. The rectenna is first characterized on a phantom body using a container of saline solution. The conductivity of the solution is taken to

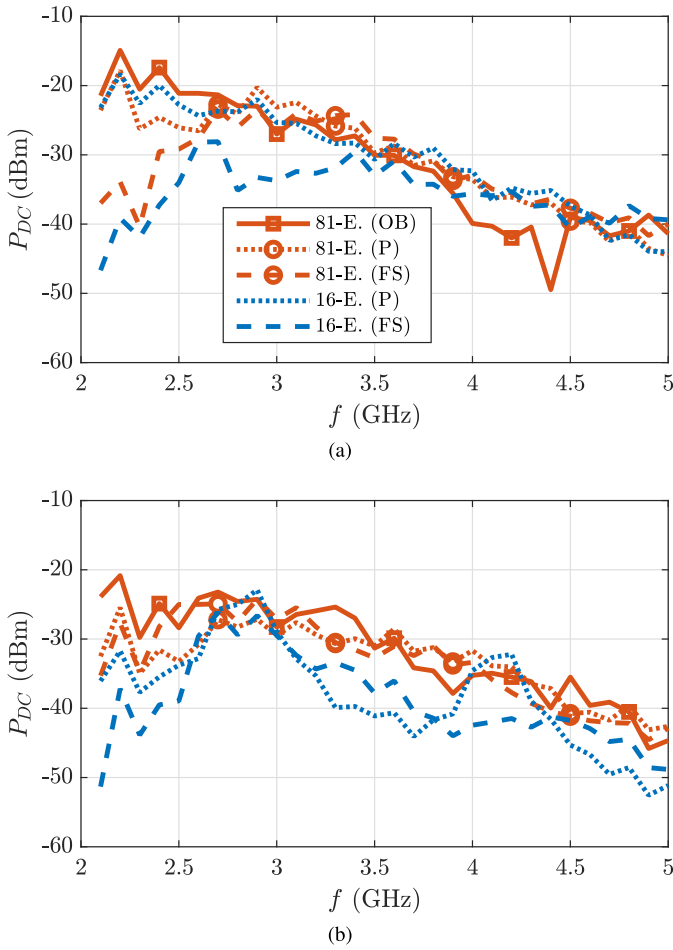


Fig. 21. Rectified dc power versus frequency for the 16- and 81-element arrays measured on-body (OB), with a phantom (P) and in free space (FS) for both (a) horizontal and (b) vertical polarization. The incident power density is  $4 \mu\text{W}/\text{cm}^2$  and dc load is  $2 \text{ k}\Omega$ .

be the weighted average of the human tissues at 2.9 GHz as given in [41], with the cross Section of the setup shown in Fig. 8(b). The photograph in Fig. 18 shows the setup in the anechoic chamber, detail of the phantom, as well as detail of a single array element.

The rectenna arrays are characterized in an anechoic chamber using the setup sketched in Fig. 19 where the tee-shirt is mounted on the phantom and the dc output is connected to a variable load. A power calibration is performed up to the plane of the transmit antenna to determine incident power on the transmit antenna as a function of RF source power and frequency. The incident power density on the rectenna array is then estimated with a well-characterized linearly polarized transmit antenna using Friis' line-of-sight equation. The energy harvester and transmit antenna are in each other's far fields at the lowest frequency of interest ( $d = 69 \text{ cm}$ ). The power available at the antenna port is calibrated and the resulting power density incident on the rectenna array is varied from 3 to  $130 \mu\text{W}/\text{cm}^2$  at each frequency point between 2 and 5 GHz in 100-MHz steps.

The dc load is varied between  $100 \Omega$  and  $5 \text{ k}\Omega$ . The dc power is measured as a function of frequency, incident

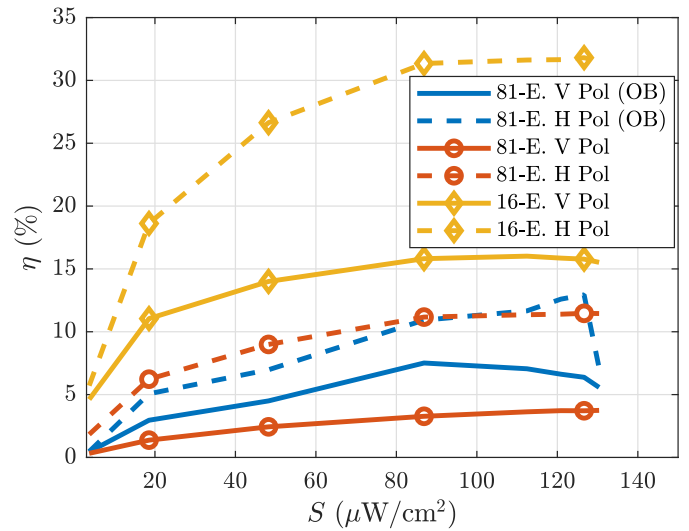


Fig. 22. Measurement results of efficiency versus incident power density at 2.9 GHz with a dc load of  $2 \text{ k}\Omega$ , showing that the fairly large resistance of the conductive ink reduces efficiency for larger arrays. On-body (OB) and on-phantom measurements are shown.

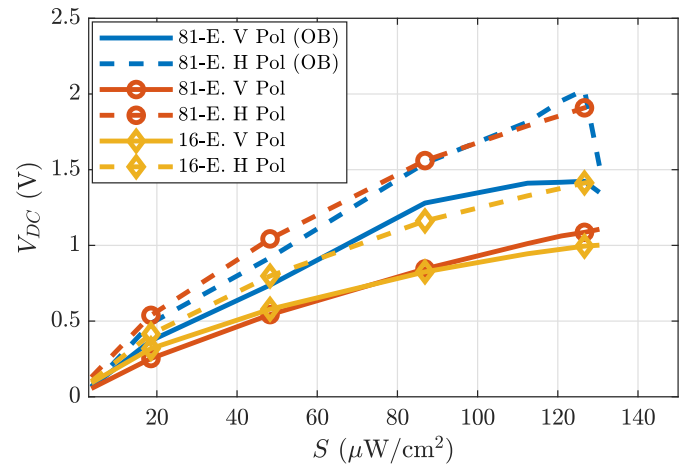


Fig. 23. Output dc voltage versus incident power density at 2.9 GHz with a dc load of  $2 \text{ k}\Omega$ . On-body (OB) and on-phantom measurements are shown.

power density, and dc load. Results showing the optimal load resistances for both polarizations are shown in Fig. 20. It is seen that for lower power levels, the optimal load is large. In addition, the load is different for the two polarizations, which is related to the antenna gain. Importantly, we observe that the power is not very sensitive to the load resistance. The extensive characterization as a function of dc load is important information for design of the power management circuit, which is typically based on a boost converter that emulates the optimal load over various power levels, as in [33]. Although here we do not focus on the power management, all relevant rectenna array characterization is performed and presented, and previously published approaches [43] can be directly applied.

Fig. 21 displays measured results for 16-element and 81-element bow-tie rectenna arrays for the two polarizations and as a function of frequency with and without the body phan-

tom. Output dc voltage,  $V_{dc}$ , and power,  $P_{dc}$ , were measured using a multimeter placed in parallel with a variable resistive load connected to the rectenna array. Several conclusions can be made. As expected, the phantom does not significantly affect the rectified power level due to the air gap and container thickness which reduce loading by the saline. Second, the horizontal polarization [referring to Fig. 21(a)] gives a higher dc output, as expected from the radiation pattern. Third, the 81-element array does not produce significantly higher power when compared with the smaller array. It is believed that the efficiency drops due to the relatively high dc resistivity of the conductive ink, which becomes more dominant as the array is scaled up in size. Conversion efficiency is defined as

$$\eta = \frac{P_{dc}}{S(0^\circ, 0^\circ) \cdot A}$$

where  $A$  is the geometric area of the arrays, which results in a conservative efficiency estimate. Fig. 22 shows the comparison between the two arrays for both polarizations. This indicates that in terms of efficiency, it is better to combine the power of several small arrays than to create a single large array. Fig. 23 shows dc output voltages for various power densities, polarizations, and array sizes.

## VI. CONCLUSION

This article presents 16- and 81-element broadband bow-tie rectenna arrays screen printed on a cotton tee-shirt for harvesting 4–130- $\mu\text{W}/\text{cm}^2$  power densities between 2 and 5 GHz. Source-pull diode simulations over a large range of dc resistances and input powers are performed to predict rectifier impedance. It is found that for lower input power levels, a larger dc load gives better efficiency. Full-wave antenna simulations are performed with specific tissue electrical parameters for the torso, as well as for a body phantom. The tightly coupled array is investigated as a function of finite size, port terminations, and separation of fabric above body. When the input impedance is simulated for the center element of a FA, it is found that the rectifier diode complex impedance termination of all other ports results in the best match to the diode source-pull impedance. For air gaps between the fabric and skin larger than 1 mm, there is little variation in the impedance and radiation pattern. In addition, simulations are performed for arrays with body curvature taken into account showing small changes in performance.

We found that screen printing on fabric with conductive ink can be used for functional rectenna array harvesters, despite the fairly large surface resistance of the ink. Silver paint was found to be a reliable method for connecting surface-mount diodes to a conductive fabric substrate and is shown to withstand hand washing in water. Measurements using a saline-filled phantom show up to  $P_{dc} = 32 \mu\text{W}$  for incident power densities of 4  $\mu\text{W}/\text{cm}^2$ , with a dc load of  $R_{dc} = 2 \text{k}\Omega$ . The measurements on the phantom compare well with those obtained with the tee-shirt rectenna worn on an actual body. For low incident power densities, the efficiency is in the 5%–10% range, and reaches 32% for 100  $\mu\text{W}/\text{cm}^2$ . Although the bow-tie array is the same for two linear polarizations,

the diode orientation gives a preferred polarization, which is clearly seen in simulations and measurements. This approach can be extended to dual polarization by adding diodes to the remaining feedpoints.

## ACKNOWLEDGMENT

The authors are grateful to Andy Fasig from Jim Morris Environmental T-Shirt Company for helpful discussions regarding the screen printing process.

## REFERENCES

- [1] L. Zhu, H.-S. Hwang, E. Ren, and G. Yang, "High performance MIMO antenna for 5G wearable devices," in *Proc. IEEE Int. Symp. Antennas Propag. USNC/URSI Nat. Radio Sci. Meeting*, Jul. 2017, pp. 1869–1870.
- [2] N. P. Basta, E. A. Falkenstein, and Z. Popovic, "Bow-tie rectenna arrays," in *Proc. IEEE Wireless Power Transf. Conf. (WPTC)*, May 2015, pp. 1–4.
- [3] J. Wang, M. Leach, E. G. Lim, Z. Wang, R. Pei, and Y. Huang, "An implantable and conformal antenna for wireless capsule endoscopy," *IEEE Antennas Wireless Propag. Lett.*, vol. 17, no. 7, pp. 1153–1157, Jul. 2018.
- [4] D. Gaetano *et al.*, "Insole antenna for on-body telemetry," *IEEE Trans. Antennas Propag.*, vol. 63, no. 8, pp. 3354–3361, Aug. 2015.
- [5] A. Cihangir, F. Gianesello, and C. Luxey, "Dual-antenna concept with complementary radiation patterns for eyewear applications," *IEEE Trans. Antennas Propag.*, vol. 66, no. 6, pp. 3056–3063, Jun. 2018.
- [6] S. J. Chen, T. Kaufmann, D. C. Ranasinghe, and C. Fumeaux, "A modular textile antenna design using snap-on buttons for wearable applications," *IEEE Trans. Antennas Propag.*, vol. 64, no. 3, pp. 894–903, Mar. 2016.
- [7] A. Kiourti, C. Lee, and J. L. Volakis, "Fabrication of textile antennas and circuits with 0.1 mm precision," *IEEE Antennas Wireless Propag. Lett.*, vol. 15, pp. 151–153, 2016.
- [8] S.-H. Li and J.-S. Li, "Smart patch wearable antenna on jeans textile for body wireless communication," in *Proc. 12th Int. Symp. Antennas, Propag. EM Theory (ISAPE)*, Dec. 2018, pp. 1–4.
- [9] H. Lee, J. Tak, and J. Choi, "Wearable antenna integrated into military berets for Indoor/Outdoor positioning system," *IEEE Antennas Wireless Propag. Lett.*, vol. 16, pp. 1919–1922, 2017.
- [10] X. Chen, H. He, Y. Lu, H. Lam, L. Ukkonen, and J. Virkki, "Fabrication and reliability evaluation of passive UHF RFID t-shirts," in *Proc. Int. Workshop Antenna Technol. (iWAT)*, Mar. 2018, pp. 1–4.
- [11] M. L. Scarpello, I. Kazani, C. Hertleer, H. Rogier, and D. Vande Ginste, "Stability and efficiency of screen-printed wearable and washable antennas," *IEEE Antennas Wireless Propag. Lett.*, vol. 11, pp. 838–841, 2012.
- [12] R. Salvado, C. Loss, R. Gonçalves, and P. Pinho, "Textile materials for the design of wearable antennas: A survey," *Sensors*, vol. 12, no. 11, pp. 15841–15857, 2012. [Online]. Available: <http://www.mdpi.com/1424-8220/12/11/15841>
- [13] J. C. G. Matthews and G. Pettitt, "Development of flexible, wearable antennas," in *Proc. 3rd Eur. Conf. Antennas Propag.*, Mar. 2009, pp. 273–277.
- [14] L. Corchia, G. Monti, and L. Tarricone, "Wearable antennas: Nontextile versus fully textile solutions," *IEEE Antennas Propag. Mag.*, vol. 61, no. 2, pp. 71–83, Apr. 2019.
- [15] N. Shinohara, *Wireless Power Transfer: Theory, Technology, and Applications*. Edison, NJ, USA: IET, 2018.
- [16] S.-E. Adami, D. Zhu, Y. Li, E. Mellios, B. H. Stark, and S. Beeby, "A 2.45 GHz rectenna screen-printed on polycotton for on-body RF power transfer and harvesting," in *Proc. IEEE Wireless Power Transf. Conf. (WPTC)*, May 2015, pp. 1–4.
- [17] C.-H. Lin, C.-W. Chiu, and J.-Y. Gong, "A wearable rectenna to harvest low-power RF energy for wireless healthcare applications," in *Proc. 11th Int. Congr. Image Signal Process., Biomed. Eng. Informat. (CISP-BMEI)*, Oct. 2018, pp. 1–5.
- [18] D. Vital, S. Bhardwaj, and J. L. Volakis, "A 2.45 GHz RF power harvesting system using textile-based single-diode rectennas," in *IEEE MTT-S Int. Microw. Symp. Dig.*, Jun. 2019, pp. 1313–1315.
- [19] G. Monti, L. Corchia, and L. Tarricone, "UHF wearable rectenna on textile materials," *IEEE Trans. Antennas Propag.*, vol. 61, no. 7, pp. 3869–3873, Jul. 2013.

- [20] R. M. E. Khosht *et al.*, "A foldable textile-based broadband archimedean spiral rectenna for RF energy harvesting," in *Proc. 16th Medit. Microw. Symp. (MMS)*, Nov. 2016, pp. 1–4.
- [21] A. Galoic, B. Ivsic, D. Bonefacic, and J. Bartolic, "Wearable energy harvesting using wideband textile antennas," in *Proc. 10th Eur. Conf. Antennas Propag. (EuCAP)*, Apr. 2016, pp. 1–5.
- [22] J. A. Hagerty, F. B. Helmbrecht, W. H. McCalpin, R. Zane, and Z. B. Popovic, "Recycling ambient microwave energy with broad-band rectenna arrays," *IEEE Trans. Microw. Theory Techn.*, vol. 52, no. 3, pp. 1014–1024, Mar. 2004.
- [23] R. Shigeta *et al.*, "Ambient RF energy harvesting sensor device with Capacitor-Leakage-Aware duty cycle control," *IEEE Sensors J.*, vol. 13, no. 8, pp. 2973–2983, Aug. 2013.
- [24] S.-M. Wu, J.-R. Yang, and T.-Y. Liu, "A transponder IC for wireless identification systems," in *Proc. 7th Int. Symp. Pers., Indoor, Mobile Commun. (PIMRC)*, vol. 1, 1996, pp. 238–241.
- [25] J. Estrada, P. Zurek, and Z. Popovic, "Harvesting of aircraft radar altimeter sidelobes for low-power sensors," in *Proc. Int. Appl. Comput. Electromagn. Soc. Symp. (ACES)*, Mar. 2018, pp. 1–2.
- [26] C. Song *et al.*, "A novel quartz clock with integrated wireless energy harvesting and sensing functions," *IEEE Trans. Ind. Electron.*, vol. 66, no. 5, pp. 4042–4053, May 2019.
- [27] A. Costanzo, D. Masotti, and M. Del Prete, "Wireless power supplying flexible and wearable systems," in *Proc. 7th Eur. Conf. Antennas Propag. (EuCAP)*, Apr. 2013, pp. 2843–2846.
- [28] M. Pinuela, P. D. Mitcheson, and S. Lucyszyn, "Ambient RF energy harvesting in urban and semi-urban environments," *IEEE Trans. Microw. Theory Techn.*, vol. 61, no. 7, pp. 2715–2726, Jul. 2013.
- [29] R. Scheeler, S. Korhummel, and Z. Popovic, "A dual-frequency ultralow-power efficient 0.5-g rectenna," *IEEE Microw. Mag.*, vol. 15, no. 1, pp. 109–114, Jan. 2014.
- [30] I. Ramos and Z. Popovic, "A compact 2.45 GHz, low power wireless energy harvester with a reflector-backed folded dipole rectenna," in *Proc. IEEE Wireless Power Transf. Conf. (WPTC)*, May 2015, pp. 1–3.
- [31] C. R. Valenta and G. D. Durgin, "Harvesting wireless power: Survey of energy-harvester conversion efficiency in far-field, wireless power transfer systems," *IEEE Microw. Mag.*, vol. 15, no. 4, pp. 108–120, Jun. 2014.
- [32] E. Falkenstein, M. Roberg, and Z. Popovic, "Low-power wireless power delivery," *IEEE Trans. Microw. Theory Techn.*, vol. 60, no. 7, pp. 2277–2286, Jul. 2012.
- [33] Z. Popovic, E. A. Falkenstein, D. Costinett, and R. Zane, "Low-power far-field wireless powering for wireless sensors," *Proc. IEEE*, vol. 101, no. 6, pp. 1397–1409, Jun. 2013.
- [34] J. Antonio Estrada *et al.*, "An octave bandwidth RF harvesting tee-shirt," in *Proc. IEEE Wireless Power Transf. Conf. (WPTC)*, London, U.K., Jun. 2019, pp. 232–235.
- [35] C. R. Paul, *Introduction to Electromagnetic Compatibility*. Hoboken, NJ, USA: Wiley, 2006.
- [36] Avago. (2007). *Application Note 1124: Linear Models for Diode Surface Mount Packages*. original document from Avago Technologies. [Online]. Available: [https://docs.broadcom.com/wcs-public/products/application-notes/application-note/829/290/av02-0038en-an\\_1124-21jul10.pdf](https://docs.broadcom.com/wcs-public/products/application-notes/application-note/829/290/av02-0038en-an_1124-21jul10.pdf)
- [37] Skyworks. (2018). *SMS7630*. original document from Skyworks Solutions. [Online]. Available: [https://www.skyworksinc.com/media/Skyworks/Documents/Products/201-300/Surface\\_Mount\\_Schottky\\_Diodes\\_200041AE.pdf](https://www.skyworksinc.com/media/Skyworks/Documents/Products/201-300/Surface_Mount_Schottky_Diodes_200041AE.pdf)
- [38] *Technical Specification Group Radio Access Network; NR; Base Station (BS) Radio Transmission and Reception (Release 15)*, 3rd Generation Partnership Project Standard, Sep. 2018.
- [39] ICNIRP, "Guidelines for limiting exposure to time-varying electric, magnetic and electromagnetic fields (up to 300 GHz)," *Health Phys.*, vol. 74, no. 4, pp. 494–522, Oct. 1998.
- [40] S. Dunbar and Z. Popović, "Low-power electronics for energy harvesting sensors," *Wireless Power Transf.*, vol. 1, no. 1, pp. 35–43, Mar. 2014.
- [41] C. Gabriel, "Compilation of the dielectric properties of body tissues at RF and microwave frequencies," Dept. Phys., King's College London, London, U.K., Tech. Rep. AL/OE-TR-1996-0037, 1996.
- [42] *Jim Morris Environmental T-Shirts*. Accessed: Jan. 7, 2019. [Online]. Available: <https://www.jimmorris.com/>
- [43] T. Paing, J. Shin, R. Zane, and Z. Popovic, "Resistor emulation approach to low-power RF energy harvesting," *IEEE Trans. Power Electron.*, vol. 23, no. 3, pp. 1494–1501, May 2008.



**José Antonio Estrada** (Member, IEEE) received the B.S. degree in electrical engineering from the University of Carabobo, Valencia, Venezuela, in 2012, and the M.S. degree in electrical engineering from the University of Colorado at Boulder, Boulder, CO, USA, in 2017, where he is currently pursuing the Ph.D. degree in electrical engineering.

He was an Assistant Lecturer with the University of Carabobo from 2012 to 2015 and was a Researcher with the Applied Electromagnetics Laboratory, Fundación Instituto de Ingeniería, Caracas, Venezuela, from 2014 to 2015, working as a Laboratory Coordinator, leading research projects and overseeing EMC compliance and antenna testing. His research interests include design of high-efficiency power amplifiers, microwave filters, tuneable RF front ends, front-end miniaturization, heterogeneous integration, energy harvesting, and wireless powering.



**Eric Kwiatkowski** (Member, IEEE) received the B.S. degree in electrical engineering from Bucknell University, Lewisburg, PA, USA, in 2015, and the M.S. degree in electrical engineering from the University of Colorado at Boulder, Boulder, CO, USA, in May 2020.

He was an Electromagnetic Design Engineer working on low-loss inductor design for consumer wireless charging applications at Pi Charging from 2016 to 2018 and was a Manufacturing Test Engineer with Lutron Electronics Inc., Coopersburg, PA, USA, from 2015 to 2016. In 2020, he joined Apple Inc., CA, USA, as an RF Systems Hardware Engineer. His research is focused on the application of array theory to nonlinear rectifying elements for wireless power applications.



**Ana López-Yela** was born in Madrid, Spain, in 1991. She received the B.S. degree in electrical engineering from the Technical University of Madrid (UPM), Madrid, in 2013, and the M.S. degree in telecommunications engineering and multimedia and communications from the University Carlos III of Madrid (UC3M), Madrid, in 2015, where she is currently pursuing the Ph.D. degree through the scholarship by the Spanish Ministry of Education, Culture and Sport under a pre-doctoral contract for University Teacher Training (FPU).

From 2015 to 2016, she worked in the MANA project for miniaturizing antennas for military aircrafts (project in collaboration with Airbus Defense and Space). During these years, she has authored or coauthored nine conferences papers (national and international) and two journal articles. Her work is divided into two different branches: on electrically small antennas for aircraft communications and in the analysis of multiple-tone receivers for energy harvesting applications.



**Mónica Borgoños-García** received the B.S. degree in electrical engineering from the Technical University of Cartagena (UPCT), Murcia, Spain, in 2017, and the M.S. degree in telecommunications engineering and in multimedia and communications from the University Carlos III of Madrid (UC3M), Madrid, Spain, in 2019.

In this time, she has authored or coauthored three conference papers (national and international). Her current work is focused on the design and implementation of wearable rectennas for wireless power transfer and energy harvesting applications.



**Daniel Segovia-Vargas** (Member, IEEE) received the Telecommunications Engineering degree and the Ph.D. degree in telecommunications engineering from the Escuela Técnica Superior de Ingenieros de Telecomunicación (ETSIT), UPM, Madrid, Spain, in 1993 and 1998, respectively.

From 1993 to 1998, he was an Assistant Professor with the Universidad de Valladolid, Valladolid, Spain. In 1998, he joined the Carlos III University of Madrid (UC3M), Madrid, where is currently a Full Professor. He has been a Visiting Researcher with

the Rutherford Appleton Laboratory, Oxfordshire, U.K. He has authored or coauthored more than 300 publications in scientific journals and international conferences (more than 80 in indexed international journals and more than 20 in international invited conferences). His current research interests include antennas (where he is currently leading a project in Airbus on antenna miniaturization for aircraft applications), active antennas, metamaterials, and technologies in THz frequencies.

Dr. Segovia-Vargas has been a member of the AP-S Society since 1998 and the MTT-S Society since 2001. He received the COIT-Ericsson Award for the best Ph.D. thesis. He has been the Treasurer of the European Microwave Conference since 2018. He was the President and Organizer of URSI2011 and a member of the Organizing Committee of EuCAP 2010 (Awards Committee). On the future EuCAP 2022, he has organized several international workshops in the domain of metamaterials and THz technologies. He has been the National Delegate for the European Cost Actions in the antennas field (Cost 284, Cost IC0603, and Cost IC1102) since 2002. He has chaired more than 70 research and development projects, both public and private.



**Taylor Barton** (Senior Member, IEEE) received the Sc.B., M.Eng., E.E., and Sc.D. degrees from the Massachusetts Institute of Technology, Cambridge, MA, USA, in 2006, 2008, 2010, and 2012, respectively.

She was a Post-Doctoral Associate with MIT Microsystems Technology Laboratories, and an Assistant Professor with The University of Texas at Dallas, Richardson, TX, USA. In 2016, she joined the Department of Electrical, Computer, and Energy Engineering, University of Colorado at Boulder,

Boulder, CA, USA, where she is currently an Assistant Professor.

Dr. Barton was a recipient of the AFOSR Young Investigator Award and the NSF CAREER Award. She holds a Lockheed Martin Faculty Fellowship with the University of Colorado at Boulder.



**Zoya Popović** (Fellow, IEEE) received the Dipl.Ing. degree from the University of Belgrade, Belgrade, Serbia, in 1985, and the Ph.D. degree from Caltech, Pasadena, CA, USA, in 1990.

She is currently a Distinguished Professor and the Lockheed Martin Endowed Chair of electrical engineering with the University of Colorado at Boulder, Boulder, CO, USA. She was a Visiting Professor with the Technical University of Munich, Munich, Germany, in 2001 and 2003, ISAE, Toulouse, France, in 2014, and the Chair of Excel-

lence at Carlos III University in Madrid, Madrid, Spain, in 2018 and 2019. She has graduated over 60 Ph.D. students and currently advises 11 doctoral students. Her research interests are in high-efficiency power amplifiers and transmitters, microwave and millimeter-wave high-performance circuits for communications and radar, medical applications of microwaves, millimeter-wave and THz quasi-optical techniques, and wireless powering.

Dr. Popović was a recipient of two IEEE MTT Microwave Prizes for best journal papers, the White House NSF Presidential Faculty Fellow Award, the URSI Issac Koga Gold Medal, the ASEE/HP Terman Medal, and the German Humboldt Research Award. She was elected as a Foreign Member of the Serbian Academy of Sciences and Arts in 2006. She was named the IEEE MTT Distinguished Educator in 2013 and the University of Colorado Distinguished Research Lecturer in 2015.